



Contents lists available at ScienceDirect

Bioorganic & Medicinal Chemistry

journal homepage: www.elsevier.com/locate/bmc

Synthesis and pharmacological characterization of a new series of 5,7-disubstituted-[1,2,4]triazolo[1,5-*a*][1,3,5]triazine derivatives as adenosine receptor antagonists: A preliminary inspection of ligand–receptor recognition process

Giorgia Pastorin^a, Stephanie Federico^b, Silvia Paoletta^c, Marta Corradino^c, Francesca Cateni^b, Barbara Cacciari^d, Karl-Norbert Klotz^e, Zhan-Guo Gao^f, Kenneth A. Jacobson^f, Giampiero Spalluto^{b,*}, Stefano Moro^{c,*}

^a Department of Pharmacy, National University of Singapore, Block S4, 18 Science Drive 4, Singapore

^b Dipartimento di Scienze Farmaceutiche, Università degli Studi di Trieste, Piazzale Europa 1, I-34127 Trieste, Italy

^c Molecular Modeling Section (MMS), Dipartimento di Scienze Farmaceutiche, Università di Padova, Via Marzolo 5, I-35131 Padova, Italy

^d Dipartimento di Scienze Farmaceutiche, Università degli Studi di Ferrara, Via Fossato di Mortara 17-19, I-44100 Ferrara, Italy

^e Institut für Pharmakologie und Toxikologie, Universität Würzburg, Versbacher Str. 9, D-97078 Würzburg, Germany

^f Molecular Recognition Section (MRS), Laboratory of Bioorganic Chemistry, National Institute of Diabetes and Digestive and Kidney Diseases, National Institutes of Health, Bethesda, MD 20892, USA

ARTICLE INFO

Article history:

Received 4 December 2009

Revised 17 February 2010

Accepted 21 February 2010

Available online 25 February 2010

Keywords:

G Protein-coupled receptors

Adenosine receptor antagonists

Triazolo-triazine

Ligand–receptor modeling studies

ABSTRACT

A new series of triazolotriazines variously substituted at the C5 and N7 (**5–25**) positions was synthesized and fully characterized at the four adenosine receptor (AR) subtypes. In particular, arylacetyl or arylcarbamoyl moieties were introduced at the N7 position, which enhanced affinity at the hA_{2B} and hA₃ ARs, respectively, when utilized on the pyrazolo-triazolopyrimidine nucleus as we reported in the past. In general, compounds with a free amino group at the 7 position (**5, 6**), showed good affinity at the rat (r) A_{2A} AR (range 18.3–96.5 nM), while the introduction of a phenylcarbamoyl moiety at the N7 position (**12, 19, 24**) slightly increased the affinity at the hA₃ AR (range 311–633 nM) with respect to the unsubstituted derivatives. The binding profiles of the synthesized analogues seemed to correlate with the substitutions at the C5 and N7 positions. At the hA_{2B} AR, derivative **5**, which contained a free amino group at the 7 position, was the most potent (EC₅₀ 3.42 μM) and could represent a starting point for searching new non-xanthine hA_{2B} AR antagonists. Molecular models of the rA_{2A} and hA₃ ARs were constructed by homology to the recently reported crystallographic structure of the hA_{2A} AR. A preliminary receptor-driven structure–activity relationship (SAR) based on the analysis of antagonist docking has been provided.

© 2010 Elsevier Ltd. All rights reserved.

Abbreviations: GPCRs, G protein-coupled receptors; AR, adenosine receptor; ADA, adenosine deaminase; cAMP, cyclic adenosine monophosphate; h, human; SAR, structure–affinity relationship; r, rat; DPCPX, 8-cyclopentyl-1,3-dipropyl-xanthine; CGS 21680, 2-[4-(2-carboxyethyl)phenethyl]amino-5'-(N-ethylcarbamoyl)adenosine; 1-AB-MECA, N⁶-(4-amino-3-iodobenzyl)-5'-(N-methylcarbamoyl)adenosine; NECA, 5'-(N-ethyl-carboxamido)adenosine; CI-IB-MECA, 2-chloro-N⁶-(3-iodobenzyl)-5'-(N-methylcarbamoyl)adenosine; TM, transmembrane; RMSD, root mean square deviation; EL2, second extracellular loop; MOE, molecular operating environment; ZM241385, 4-(2-[7-amino-2-[2-furyl]{1,2,4}triazolo(2,3-a){1,3,5}triazin-5-yl amino]ethyl)phenol.

* Corresponding authors. Tel.: +39 040 6762525; fax: +39 040 52572 (G.S.); tel.: +39 049 8275704; fax: +39 049 8275366 (S.M.).

E-mail addresses: spalluto@univ.trieste.it (G. Spalluto), stefano.moro@unipd.it (S. Moro).

1. Introduction

Activation or blockade of adenosine receptors (ARs) is responsible for a broad range of effects in various organ systems suggesting that regulation of ARs has substantial therapeutic potential. Recent the focus has been increased on the cardioprotective^{1,2} and neuro-protective^{3,4} effects associated with AR activation during periods of cardiac and cerebral ischemia, respectively. It has also been proposed that antagonists of distinct AR subtypes may be used in the treatment of asthma^{5,6} or certain neurological diseases such as Parkinson's disease.^{6,7} A complete summary of the physiological roles of ARs and their potential as clinical targets in a variety of disease states have been recently reported.^{6–11}

All ARs are members of the superfamily of G protein-coupled receptors (GPCRs), with four subtypes currently recognized, the A₁AR, A_{2A}AR, A_{2B}AR, and A₃AR,¹² which exert their physiological

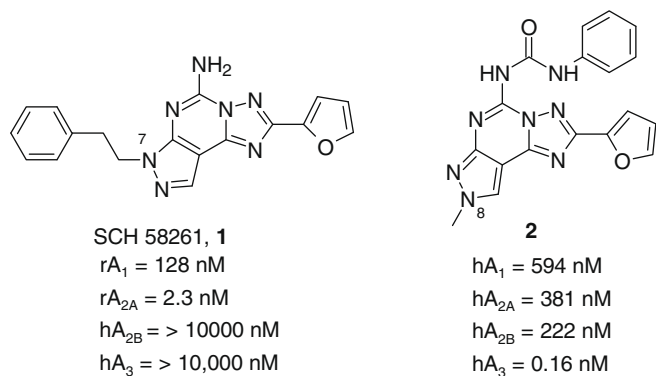


Chart 1. Pyrazolo-triazolopyrimidine derivatives as A_{2A} and A_3 AR antagonists.

role by activation or inhibition of several second messenger systems. In particular, the modulation of adenylate cyclase activity could be considered to be the principal signal mediated by these receptors.^{1,2}

In the last 20 years intense medicinal chemical efforts led to the synthesis of a variety of AR agonists and antagonists for the pharmacological characterization of this family of G protein-coupled receptors.¹³ With respect to antagonists, several classes of heterocyclic derivatives have been reported as AR antagonists with high levels of both affinity and selectivity. In particular, in recent years we investigated in depth the nucleus of triazolo-pyrazolopyrimidine as a basis for designing ARs antagonists. Modulating the substitution at the C5, N7 and N8 positions (Chart 1) led to potent and selective A_{2A} and A_3 AR antagonists (compounds **1** and **2**).^{14–21}

Nevertheless, this class of compounds, like other tricyclic structures, was subject to poor water solubility and more importantly complicated synthetic routes. In consideration of these problems, medicinal chemists recently focused their attention on the synthesis of more simplified heterocyclic derivatives, in particular bicyclic systems such as adenine,²² triazolopyrazine^{23–25} and triazolotriazine.^{26–28} One of the most appealing bicyclic cores is represented by the triazolotriazine nucleus, which led in the past to the discovery of ZM241385 (**3**) that could be considered as one of the most potent A_{2A} AR antagonists yet reported.^{29,30} In addition, **3** also binds with high affinity at the human (h) A_{2B} AR (28 nM), and its tritiated form is suitable for use as a radioligand in binding studies at this receptor subtype.³¹ Very recently a large number of triazolotriazine derivatives bearing different substitution at the 5-position have been reported,²⁶ and compound **4** proved to be potent and selective for the A_{2A} in comparison to the A_1 AR. Nevertheless, the lack of binding data at the A_{2B} and A_3 ARs prevents a comparison with other fully characterized derivatives (Chart 2).²⁶

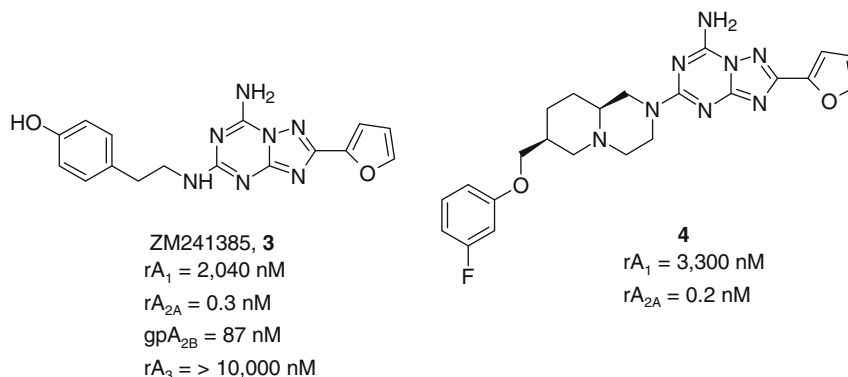


Chart 2. Triazolotriazine derivatives as AR antagonists.

Taking into account these experimental observations, we decided to better investigate the potential of modifying this nucleus at the C5 and N7 positions (**5–25**). In particular, arylacetyl or arylcarbonyl moieties at the N7 position on the pyrazolo-triazolopyrimidine nucleus enhanced affinity at the A_{2B} and A_3 ARs, respectively (Chart 3).^{17,21}

All the compounds have been fully characterized at the four ARs with the aim of better understanding the structure–activity relationship (SAR) profile of this class of compounds and optimizing the substitution in order to modulate both AR affinity and selectivity. Moreover, a preliminary receptor-driven SAR based on the recently published crystallographic structure of the hA_{2A} AR has been provided.

2. Results and discussion

2.1. Chemistry

The compounds with the free amino group bearing a phenoxy (**5**) or methylthio (**6**) residue at the C5 position were prepared as previously described by Caulkett et al.,³² while introduction of a dimethylamino group at the C5 position (**7**) was performed by heating compound **5** at 120 °C in a sealed tube with an ethanolic solution (33%) of dimethylamine.

Derivatives substituted at the N7 position (**8–25**) were prepared by treating compounds **5–7** with the appropriate acylchloride (in presence of triethylamine) or arylisocyanate in dioxane at reflux (Scheme 1).

2.2. Biological activity

The receptor binding affinities of the synthesized compounds (**5–25**) are reported in Table 1. Binding was conducted at the following ARs: rat A_1 (from rat cerebral cortex membranes),³³ rat A_{2A} (from rat striatal membranes),³⁴ and hA_3 (from HEK-293 cells expressing the hA_3 AR).³⁵ [³H]N⁶-Phenylisopropyladenosine ([³H]R-PIA), (A_1)³³ [³H]2-[4-[(2-carboxyethyl)-phenyl]ethylamino]-5'-N-ethylcarbamoyladenosine, ([³H]CGS21680) (A_{2A})²⁴ and [¹²⁵I]N⁶-(4-amino-3-iodobenzyl)-5'-N-methylcarbamoyladenosine ([¹²⁵I]I-AB-MECA) (A_3)²⁶ have been used as radioligands in binding assays. Instead, for evaluating potency at the hA_{2B} AR, due to the lack of a readily available radioligand, the activity of antagonists was determined in adenylyl cyclase experiments in CHO (Chinese hamster ovary) cells expressing the hA_{2B} AR.^{37,38}

All of the synthesized compounds showed affinities at the four ARs in the high nanomolar or micromolar range without significant levels of selectivity. The analysis of the data reported in Table 1, clearly indicates that in general, with the exception of compound

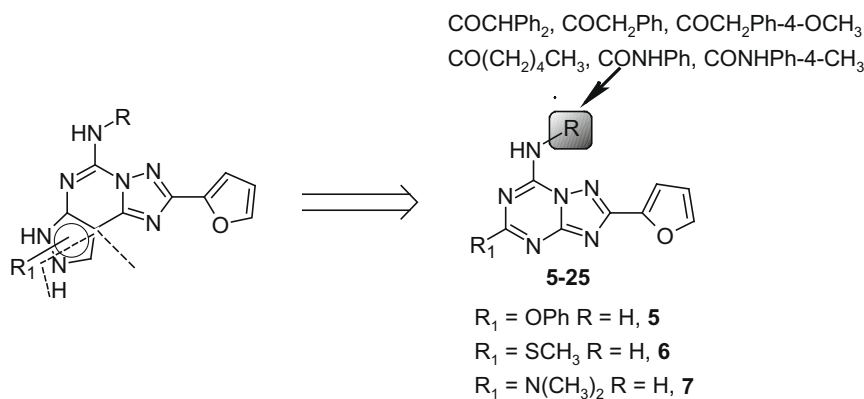
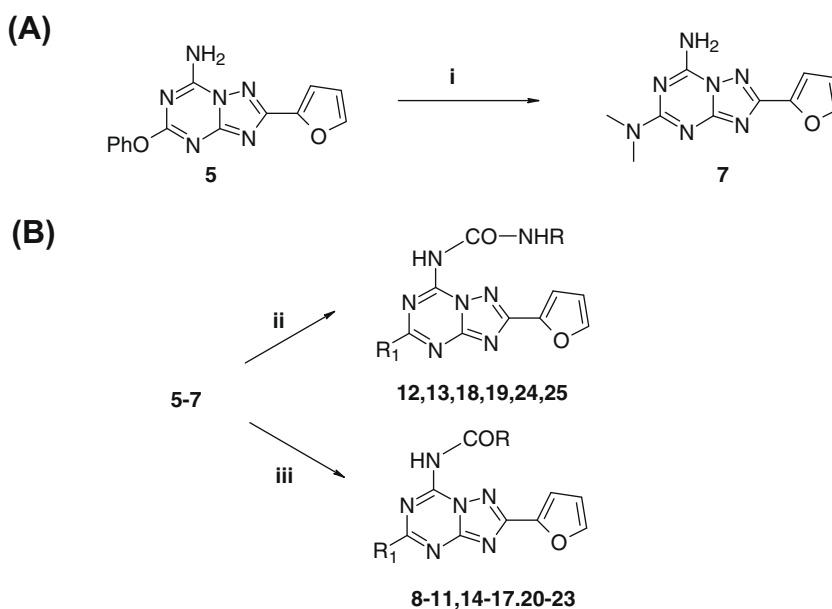


Chart 3. Molecular simplification approach applied for the design of the novel triazolotriazine analogs.



Scheme 1. Reagents: (i) EtOH, dimethylamine, 120 °C sealed tube, 4 h; (ii) R–N=C=O, dioxane, Et₃N, reflux, 12 h; (iii) R–COCl, dioxane, reflux, 12 h.

7, compounds with a free amino group at the 7 position (**5** and **6**) showed good affinity at the A_{2A} AR (range 18.3–96.5 nM) with quite significant levels of selectivity versus the other AR subtypes.

A significantly different selectivity profile could be noted when the amino group at the 7 position was substituted with an acyl group, and most importantly the affinities at the four AR subtypes seemed to be very sensitive to the substitution at both the 5 and 7 positions.

In particular, when a phenylacetyl moiety was introduced at the N7 position (**9**, **15**, and **21**) the binding profiles of the derivatives were quite different with respect to the N7 unsubstituted derivatives (**5–7**), and it was also significantly modified by the substitution at the 5 position. In fact, the presence of a methylthio (**9**) or phenoxy (**15**) group at the 5 position enhanced affinity at the A_{2A} AR (range 136–429 nM), while the potency at the other receptor subtypes was poor (range 1–7 μM). In contrast, the presence of a dimethylamino group at the 5 position (**21**) reduced affinity (1–7 μM) at all the ARs. When the phenylacetyl moiety at the N7 was substituted at the *para* position with a methoxy group (**10**, **16**, and **22**), a general decrease of affinity versus all the ARs were observed in comparison to the unsubstituted derivatives (**9**, **15**, and **21**). If a bulky arylacetyl moiety (such as diphenylacetyl-**8**, **14**, and **20**) was introduced at the N7 position, a completely different biological profile was evident. In fact, the presence of a bulky substituent at the N7, position combined with a methylthio (**8**)

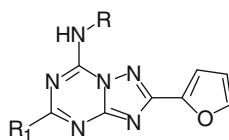
or dimethylamino (**20**) group at the 5 position, favored A₁ and A₃ ARs affinities (range 170–950 nM). In contrast, the presence of a phenoxy group at the 5 position reduced affinity at all the ARs.

Different binding affinities were observed when an acyl chain was introduced at the N7 position. In fact, a combination of an acyl chain at the N7 position with a methylthio (**11**) or a phenoxy (**17**) groups at the 5 position afforded good affinity at the A_{2A} AR (range 180–400 nM), while the affinities at the other AR subtypes was poor. However, the presence of a dimethylamino group at the 5 position (**23**) was detrimental to affinity at all the AR subtypes.

Incorporation of an arylcarbamoyl moiety at the N5 position of the pyrazolo-triazolopyrimidine nucleus (e.g., compound **2**) enhanced hA₃ AR affinity. In general, the affinity at the A₁ AR was poor (range from 3 μM to >10 μM) independent of the substitution at the 5 position (**12**, **13**, **18**, **19**, **24**, **25**). However, phenoxy (**18**, **19**) or dimethylamino (**24**) groups at the 5 position enhanced the affinity at the A_{2A} subtype (range 39–580 nM).

Thus, most of these derivatives were nearly inactive at the hA₃ AR, with the exception of compounds **12**, **18**, and **24**, which showed hA₃ affinity in the high nanomolar range (range 311–633 nM) and were characterized by the presence of an unsubstituted phenylcarbamoyl moiety at the N7 position, independently of the substitution at the N5 position. The low affinity at the hA₃ AR, was quite surprising considering that triazolotriazine

Table 1
Structures and binding profile of synthesized compounds **5–25**



5-25

#	R ¹	R	rA ₁ (K _i , nM) % displ. at 10μM ^a	rA _{2A} (K _i , nM) ^b	hA _{2B} EC ₅₀ (nM) ^c	hA ₃ (K _i , nM) or % displ. at 10μM ^d	rA ₁ /rA _{2A}	rA ₁ /hA ₃	rA _{2A} /hA ₃
5	OPh	H	2,720 ± 680	18.3 ± 3.4	3,420 ± 200	489 ± 63	148	0.04	5.5
6	SCH ₃	H	1730 ± 360	96.5 ± 36.1	14,900 ± 1,700	2580 ± 780	18	0.7	0.04
7	N(CH ₃) ₂	H	31,400 ± 8000	3800 ± 1230	33,700 ± 1,800	7270 ± 2230	8.3	4.3	0.5
8	SCH ₃	COCHPh ₂	557 ± 205	> 10,000	> 100,000	170 ± 45	< 0.05	3.2	59
9	SCH ₃	COCH ₂ Ph	1420 ± 260	429 ± 38	> 100,000	4200 ± 950	3.3	0.33	0.1
10	SCH ₃	COCH ₂ -Ph-4OCH ₃	5000 ± 1170	1570 ± 660	42,400 ± 9,900	2100 ± 400	3.2	2.4	0.7
11	SCH ₃	CO(CH ₂) ₄ CH ₃	1520 ± 170	427 ± 96	> 100,000	24 ± 3%	3.5	< 0.04	< 0.15
12	SCH ₃	CONHPh	10,000 ± 2900	1660 ± 1120	17,100 ± 2,700	414 ± 29	6	24	4
13	SCH ₃	CONH-Ph-4CH ₃	3440 ± 690	742 ± 194	16,800 ± 3,100	2200 ± 54	4.6	1.5	0.3
Compd	R ¹	R	rA ₁ (K _i , nM)	rA _{2A} (K _i , nM)	hA _{2B} EC ₅₀ (nM)	hA ₃ (K _i , nM) or% displ. at 10μM	rA ₁ /rA _{2A}	rA ₁ /hA ₃	rA _{2A} /hA ₃
14	OPh	COCHPh ₂	<10% inhib	1880 ± 310	> 100,000	4400 ± 1150	> 5.3	> 2.2	0.4
15	OPh	COCH ₂ Ph	7260 ± 2820	136 ± 48	> 100,000	1020 ± 173	53	7	0.13
16	OPh	COCH ₂ -Ph-4-OCH ₃	12 ± 2% inhib	892 ± 252	> 100,000	5200 ± 1300	> 11	> 2	0.17
17	OPh	CO(CH ₂) ₄ CH ₃	2900 ± 710	189 ± 26	> 100,000	2200 ± 470	15	1.3	0.08
18	OPh	CONHPh	17 ± 5% inhib	38.9 ± 3.5	8,870 ± 1,680	633 ± 37	> 257	> 16	0.06
19	OPh	CONH-Ph-4CH ₃	35 ± 5% inhib	214 ± 72	20,000 ± 3,600	750 ± 130	> 46	> 13	0.3
20	N(CH ₃) ₂	COCHPh ₂	951 ± 88	4090 ± 1360	> 100,000	473 ± 85	0.2	2	8.6
21	N(CH ₃) ₂	COCH ₂ Ph	6080 ± 1040	6700 ± 3200	> 100,000	1050 ± 466	0.9	5.8	6.4
22	N(CH ₃) ₂	COCH ₂ -Ph-4-OCH ₃	8740 ± 590	10,300 ± 1,300	> 100,000	2700 ± 345	0.8	3.2	3.8
23	N(CH ₃) ₂	CO(CH ₂) ₄ CH ₃	1570 ± 380	> 10,000	> 100,000	2200 ± 370	< 0.16	0.7	> 4.5
24	N(CH ₃) ₂	CONHPh	3150 ± 550	580 ± 100	> 100,000	311 ± 122	5.4	10	1.8
25	N(CH ₃) ₂	CONH-Ph-4CH ₃	2720 ± 830	2720 ± 2090	> 100,000	9600 ± 1200	1	0.3	0.3

^a Displacement of specific [³H]R-PIA binding (A₁) in rat brain membranes.

^b Displacement of specific [³H]CGS 21680 binding (A_{2A}) in rat striatal membranes.

^c Measurement of adenylyl cyclase activity in CHO cells stably transfected with human recombinant A_{2B} AR, expressed as EC₅₀ (μM).

^d Displacement of specific [¹²⁵I]-I-AB-MECA binding at hA₃ receptors expressed in CHO cells. Data are expressed as K_i ± SEM in nM or as % of displacement at 10μM (n = 3–6).

derivatives were simplified analogs of the pyrazolo-triazolopyrimidine antagonists of the hA₃ AR. Nevertheless, a careful structural analysis of these two classes of compounds, by comparing the derivatives **24** and **2**, clearly indicated that the dimethyl-amino group on the triazolotriazine nucleus is not favored. In fact, the dimethylamino group seemed not to correspond to the N8-methyl group of derivative **2**, but was similar to its N7 pattern of substitution, which was extensively demonstrated to be inactive at the hA₃ AR.^{13–15}

Regarding the activity of this series at the hA_{2B} AR, most of compounds were almost inactive at this receptor subtype. Only two compounds, bearing a phenoxy group at the 5 position (**5**, **18**), showed promising activity in the adenylyl cyclase assays at the A_{2B} AR, with an EC₅₀ ranging from 3.4 to 8.8 μM. In particular, derivative **5**, which contained a free amino group at the 7 position, was the most potent at the hA_{2B} AR, and could represent a starting point for new non-xanthine hA_{2B} AR antagonists. Nevertheless, the high potency of this compound at the A_{2A} AR (18.3 nM) clearly indicated that further investigation would be needed in order to delineate the activities at these two ARs. A summary of the most relevant structure–activity features of the novel triazolotriazine analogs has been reported in Chart 4.

2.3. Molecular modeling

It was clear from the data analysis that it was very difficult to define a robust SAR profile of this new class of compounds. For this reason and with the aim to better understand these pharmacological results, molecular modeling and docking studies have been per-

formed in parallel at the A_{2A} and A₃ ARs. Therefore, we built models of the rA_{2A} and hA₃ receptors by homology modeling, using as template the crystal structure of hA_{2A} receptor (PDB code: 3EML),³⁹ methodological details are summarized in Section 4. Figure 1 shows the alignment of the three amino acid sequences (hA_{2A}/rA_{2A} sequence identity 82%; hA_{2A}/hA₃ sequence identity 41%).

Then, we performed docking studies to recognize the hypothetical binding motif of the newly synthesized 5,7-disubstituted-[1,2,4]triazolo[1,5-a][1,3,5]triazine derivatives. We compared our docking simulation results with the docking poses of ZM241385 at both receptors. As reported in Section 4, four different programs have been used to calibrate our docking protocol using the crystallographic pose of ZM241385 into human A_{2A} as reference. Based on the lowest average ligand RMSD value obtained from the different docking algorithms, we decided to use GOLD as docking program for the pose inspection of the novel 5,7-disubstituted-[1,2,4]triazolo[1,5-a][1,3,5]triazine derivatives.

As shown in Figure 2, the binding motif of ZM241385 at the rA_{2A} receptor was similar to the crystallographic pose on the hA_{2A} receptor; this was consistent with the binding affinity of ZM241385 at the two receptors (K_i = 0.21–0.50 nM and K_i = 0.7–1.0 nM, respectively).^{40,41} Consistently, all the residues belonging to the binding pocket are conserved in both receptors. The numbering of the amino acids in parenthesis follows the numbering convention of Ballesteros and Weinstein: according to this scheme, each amino acid identifier starts with the helix number, followed by the position relative to a reference residue among the most conserved amino acid in that helix, with the reference residue arbitrarily assigned the number 50.⁴²

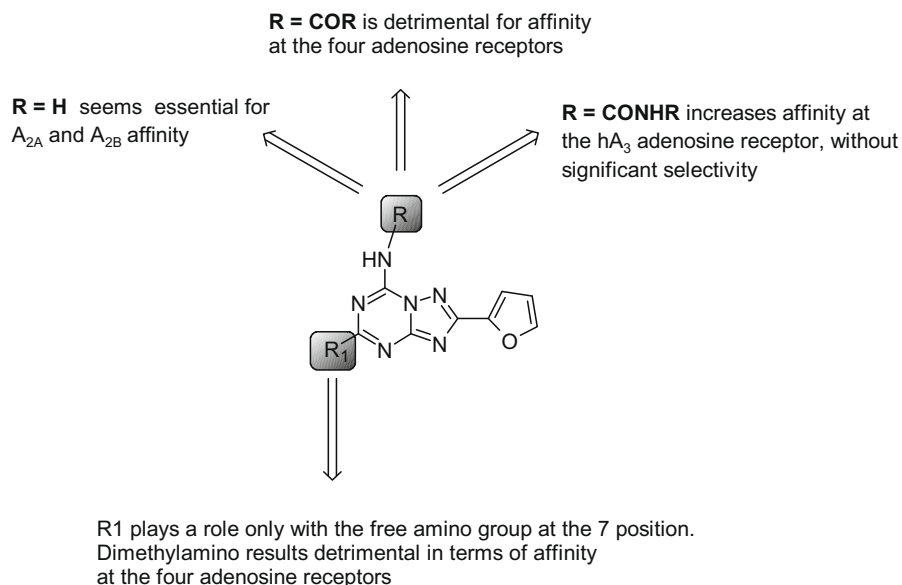


Chart 4. Summary of the most relevant SAR features of the novel triazolotriazine analogs.

	TM1	IL1	TM2	
ha2a (P29274)	MP-----IMGSSVYITVELAIAVLAAILGNVLCWAVWLNLSNLQNVNTNYFVVSLAAADIA			54
rA2a (P30543)	-----MGSSVYITVELAIAVLAAILGNVLCWAVWINSNLQNVNT FF VVSLAAADIA			51
ha3 (P33765)	MPNNSTALSLANVTYITMETFI GLCAIVGNVLCVVKLN PSLQTTTFYFIV SLALADIA			60
	* * * * *	* * * * *	* * * * *	
	EL1	TM3	IL2	
ha2a (P29274)	VGVLAI PF AITISTGFCAACHGCLFIACFVLVLTQSSIFSLLAIAIDRYIAIRIPLRYNG			114
rA2a (P30543)	VGVLAI PF AITISTGFCAACHGCL FF ACFVLVLTQSSIFSLLAIAIDRYIAIRIPLRYNG			111
ha3 (P33765)	VGVL VM PLAIVVSL GI T HF YSCL FM T CL LL IF THAS IM SLLAIAVD RY LRV KL TVRY KR			120
	* * * * *	* * * * *	* * * * *	
	TM4	EL2		
ha2a (P29274)	LVTGTRAKGIIAICWVLSFAIGLTPMLGWNNCGQPKEGKNHSQGCQEGQVACLFEDVVP			174
rA2a (P30543)	LVTG V RAKGIIAICWVLSFAIGLTPMLGWNNCSQ-KDG- NS TKTCGEG RV TCLFEDVVP			169
ha3 (P33765)	VT HRR I W L AL G LC W LV S FLVGL T PM F GW N ----- M KL T SEY H R N V T FL S C Q F V S M R M			174
	* * * * *	* * * * *	* * * * *	
	TM5	IL3	TM6	
ha2a (P29274)	NYMVYFN F ACVLVPLLLMLGVYLRIFLAARRQLKQMESQPLPGERARSTLQKEVHAAKS			234
rA2a (P30543)	NYMVY N PF F VL L PLLLML AI YLRIFLAARRQLKQMESQPLPGER T RSTLQKEVHAAKS			229
ha3 (P33765)	D Y M VY F S PL T W I F I PL V M CA IY L D I F Y I R N K L S L N L S N --- SK E T G A F Y G R E F K T A K S			231
	* * * * *	* * * * *	* * * * *	
	EL3	TM7		
ha2a (P29274)	LAIIVGLFALCWLPLHIINCF T FFCPDCSHAPLWLMYLAIIVLSHTNSVNVNPFYAYRIRE			294
rA2a (P30543)	LAIIVGLFALCWLPLHIINCF T FFC S T C RHAPP W LMYLAIILSHNSVNVNPFYAYRIRE			289
ha3 (P33765)	L F L V L F L F A L S W L P L S I IN C I I Y F N --- GE V P Q L V L V M G I L S H A N S M N P I V Y A K I K			288
	* * * * *	* * * * *	* * * * *	
ha2a (P29274)	FRQ T FRKIIRSHVLRQ Q EPFKAAGTSARVLAAHGSDGEQVSLRLNGHPGVWANGSAPHP			354
rA2a (P30543)	FRQ T FRKIIR T HVLR R Q Q EPF Q AG S S A W A L A A H S T E G EQVSLRLNGHP L GVWANGS A T H S			349
ha3 (P33765)	F K E T Y L L I L K A C V V --- ----- C H P S D S L D T S I E K N S E ---			318
	* * * * *	* * * * *	* * * * *	
ha2a (P29274)	ERRPNGYALGLVSGGSAQESQGN T GLPDVELLSHELKGVCEPPGLDDPLAQDGAGVS ---			412
rA2a (P30543)	G RRPNGY T L G L G GGGSA Q S P R --- -----D V E L P T Q E R Q - E Q E H P G L R G H L V Q A R V A S S W			403
ha3 (P33765)	-----			
ha2a (P29274)	-----			
rA2a (P30543)	SSEFAPS 410			
ha3 (P33765)	-----			

Figure 1. Multiple sequence alignment of hA_{2A} receptor, rat A_{2A} receptor and hA_3 receptor. Conserved residues in all the sequences are identified by stars. Differences in sequences of rA_{2A} and hA_3 compared to hA_{2A} are shown in *boldface type*.

From the analysis of docking of ZM241385 in the rA_{2A} AR, it appeared that the bicyclic triazolotriazine core was anchored through an aromatic stacking interaction with Phe163 (EL2), an aliphatic

hydrophobic interaction with Ile269 (7.39), and a hydrogen bonding interaction with Asn248 (6.55). The exocyclic amino group, linked to the bicyclic core of ZM241385, interacts with two polar

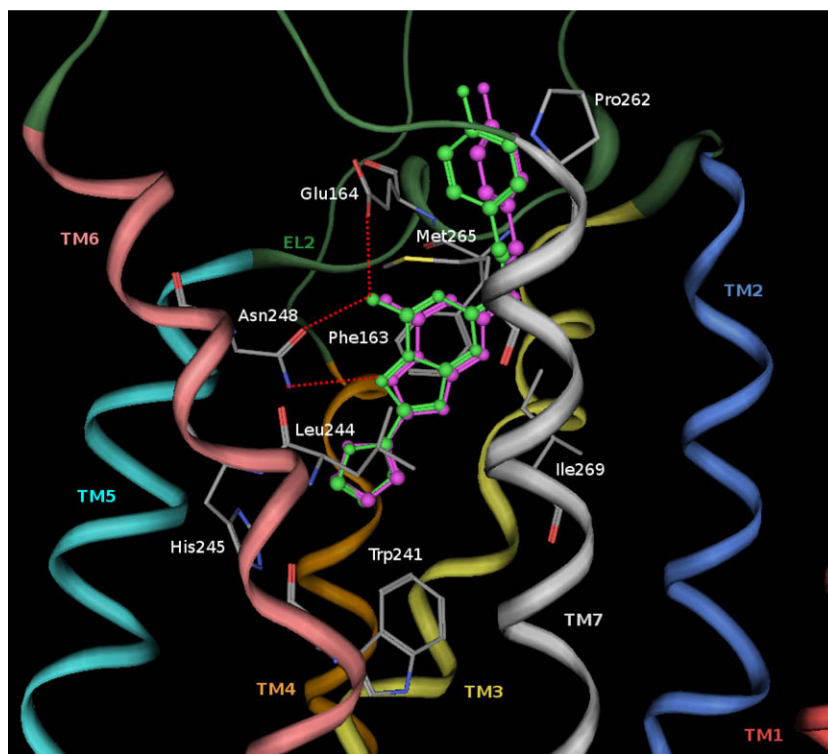


Figure 2. Structure superimposition of crystallographic pose (in magenta) and docking pose (in green) of ZM241385 inside the rA_{2A} AR binding site. Side chains of some amino acids important for ligand recognition and H-bonding interactions are highlighted. Hydrogen atoms are not displayed.

residues, Asn248 (6.55) and Glu164 (EL2). The phenyl ring forms hydrophobic interactions with Pro262 (7.32) and Met265 (7.35). The phenylethylamine substituent was directed towards the more solvent exposed extracellular region (EL2 and EL3) rather than towards the transmembrane domains of the receptor. The furan ring was located deep in the ligand binding cavity and directed towards TM5 and TM7; it forms hydrophobic interactions with the highly conserved Trp241 (6.48), an important residue in receptor activation,⁴³ His245 (6.52) and Leu244 (6.51).

The triazolotriazine derivatives with a free amino group at the 7 position (**5–7**) show a similar binding motif to ZM-241385 inside the transmembrane region of the rA_{2A} receptor, as reported in Figure 3. In particular, the three H-bonding interactions with Asn248 (6.55) and Glu164 (EL2) are conserved.

Among these, compound **5** ($K_i rA_{2A}AR = 18.3 \pm 3.4$) was the most potent because the phenoxy group forms strong hydrophobic interactions with side chains of the following residues: Leu162 (EL2), Phe163 (EL2), Pro262 (7.32), Met265 (7.35), Tyr266 (7.36) and Ile269 (7.39). Calculated $\log P$ values of compounds **6** and **7** (1.01 and -0.24 , respectively) could explain the different affinities at the receptor, even though the two R^1 substituents were not involved in particular interactions with residues of the binding pocket. The hydrogen bonding network with Asn248 (6.55) and Glu164 (EL2) seems to be critical both for the recognition of these antagonist structures and for receptor selectivity versus hA_3 . In particular, Glu164 (EL2) of rA_{2A} receptor subtype (Glu169 in hA_{2A}) was not present in the corresponding position of hA_3 receptor, where this amino acid was replaced by valine (Val169); in fact molecular docking results on hA_3 suggest that compounds **5**, **6** and **7** ($K_i hA_3AR = 489 \pm 63$, 2580 ± 780 , 7270 ± 2230 , respectively) form only two (with Asn250) of the three hydrogen bonding interactions (data not shown).

Among other compounds (**8–25**) the most potent at the rA_{2A} receptor was **18** ($K_i rA_{2A}AR = 38.9 \pm 3.5$). As shown in Figure 3, because of the presence of the phenylcarbamoyl moiety at N7, the

binding pose of compound **18** results to be quite different compared with the unsubstituted derivatives (ZM241385, **5–7**). In fact, the R substituent was directed towards TM2 and TM3 rather than towards TM5 and TM6 and was located in a hydrophobic pocket delimited by Ala56 (2.57), Ile57 (2.58), Phe59 (2.60), Ala60 (2.61), Ile63 (2.64), Phe77 (3.28), Ala78 (3.29), Phe80 (3.31) and Val81 (3.32). Nevertheless, compound **18** formed also the same hydrophobic interactions as compound **5** and ZM241385, but only one hydrogen bonding interaction with Asn248 (6.55). Moreover the bicyclic triazolotriazine core of the disubstituted ligand was aligned with the same region of the other two compounds.

In the hA_3 receptor, the presence of the less bulky side chain of Val169 (EL2) allows the phenylcarbamoyl moiety of compound **18** to direct towards TM5 and TM6 and so it loses the interactions with the residues of the hydrophobic pocket. Moreover, all the 5,7-disubstituted-[1,2,4]triazolo[1,5-*a*][1,3,5]triazine derivatives were located deeper in the ligand binding cavity of hA_3 ; consequently they lose the π - π stacking interaction with Phe168 (EL2).

With respect to the R^1 moieties, the SAR at rA_{2A} was similar for compounds **8–25** and compounds **5–7**. It seems that the presence of too bulky substituents at the N7 position was not well tolerated because of unfavourable steric interactions.

To analyze in a more quantitative way the possible ligand-receptor recognition mechanism, the individual electrostatic (ΔE_{int}^{el}) and hydrophobic (ΔE_{int}^{hyd}) contributions to the interaction energy (ΔE_{int}) of each receptor residue has been calculated (see Section 4 for more details). Analyzing the results of this study (collected in Figs. 4 and 5) it is clear that, from the electrostatic point of view, two of the most critical residues affecting the affinity at ARs seem to be the asparagine 6.55 (Asn253 in hA_{2A} , Asn248 in rA_{2A} and Asn250 in hA_3) and the glutamic acid located within EL2 of both human and rat A_{2A} (Glu169 and Glu164, respectively) but mutated in valine in hA_3 (Val169). In particular, Asn 6.55 is responsible of two stabilizing interactions with ZM241385 in both human and rat A_{2A} and this is supported by the electrostatic contribution



Figure 3. Structure superimposition of docked conformations of compound **5** (in red, K_i $rA_{2A}AR = 18.3 \pm 3.4$) and compound **18** (in magenta, K_i $rA_{2A}AR = 38.9 \pm 3.5$) inside the rA_{2A} AR binding pocket. Side chains of some amino acids important for ligand recognition and H-bonding interactions are highlighted. Hydrogen atoms are not displayed.

of around -13 kcal/mol to the whole interaction energy, in particular -9.5 kcal/mol in hA_{2A} and -17.9 kcal/mol in rA_{2A} (Fig. 4). In addition, the glutamic acid on EL2 can strongly interact through an additional hydrogen-bond with the exocyclic amino group of ZM-241385 as supported by the stabilizing electrostatic contribution of around -13 kcal/mol to the whole interaction energy, in particular -9.0 kcal/mol in hA_{2A} and -17.6 kcal/mol in rA_{2A} (Fig. 4). Consistently, this specific interaction is missing in hA_3 .

Interestingly, compound **5** presents a very similar electrostatic energy contributions to ZM241385 supporting the hypothesis of a common TM binding motif. Conversely, compound **18** completely abolishes the capability to interact with both asparagine 6.55 and glutamic acid on EL2 due to the presence of phenylcarbamoyl moiety that forces the triazolotriazine moiety to flip 180° (around its parallel TM axis) inside the TM binding cleft. However, the lack of these two stabilizing interactions seems to be balanced by the presence of several additional hydrophobic interactions as mapped in Figure 5.

In fact, besides the three hydrophobic contributions mediated by the conserved phenylalanine on EL2 (Phe168 in hA_{2A} , Phe163 in rA_{2A} and Phe168 in hA_3), the leucine 6.51 (Leu249 in hA_{2A} , Leu244 in rA_{2A} and Leu246 in hA_3) and the tryptophan 6.48 (Trp246 in hA_{2A} , Trp241 in rA_{2A} and Trp243 in hA_3), the phenylcarbamoyl moiety at N7 is surrounded by several hydrophobic side chains such as, for example for the rA_{2A} , Ala56 (2.57), Ile57 (2.58), Phe59 (2.60), Ala60 (2.61), Ile63 (2.64), Phe77 (3.28), Ala78 (3.29), Phe80 (3.31) and Val81 (3.32).

3. Conclusion

The present study has led to the identification of a new class of promising AR antagonists, the 5,7-disubstituted-[1,2,4]triazolo[1,5-*a*][1,3,5]triazine derivatives, which were designed as simplified analogues of our previously reported hA_{2A} and hA_3 antagonists. To depict the binding motif of these new AR antago-

nists, a novel model of the rA_{2A} and hA_3 receptor, based on the recently published structure of the human A_{2A} receptor, was built. These new AR models provide a self-consistent framework that rationalizes the available SAR data. Moreover, a very preliminary hypothesis, concerning the specific roles of a few crucial amino acids in affecting the molecular mechanism of both ligand-entering process and TM-recognition process, has been proposed.

4. Experimental section

4.1. Chemistry

4.1.1. General

Reactions were routinely monitored by thin-layer chromatography (TLC) on silica gel (precoated F_{254} Merck plates). Infrared spectra (IR) were measured on a Jasco FT-IR instrument. 1H NMR were determined in $CDCl_3$ or $DMSO-d_6$ solutions with a Varian Gemini 200 spectrometer, peaks positions are given in parts per million (δ) downfield from tetramethylsilane as internal standard, and J values are given in hertz. Light petroleum ether refers to the fractions boiling at 40 – 60 °C. Melting points were determined on a Buchi-Tottoli instrument and are uncorrected. Flash chromatography was performed using Merck 60–200 mesh silica gel. Elemental analyses were performed by the microanalytical laboratory of Dipartimento di Chimica, University of Trieste, and were within $\pm 0.4\%$ of the theoretical values for C, H and N.

4.1.1.1. 7-Amino-5-dimethylammino-2-(2-furyl)-[1,2,4]triazolo[1,5-*a*]-[1,3,5] triazine (7). To a solution of phenoxy derivative **5** (0.3 g, 1.01 mmol) in ethanol (5 mL) was added a large excess (5 equiv) of an ethanolic solution (33%) of dimethylamine (0.7 mL). The resulting solution was transferred to a sealed tube and heated at 120 °C for 4 h. Then the solvent was removed at reduced pressure and the crude residue purified by flash chromatography (EtOAc–light petroleum 1:1) to afford the desired product

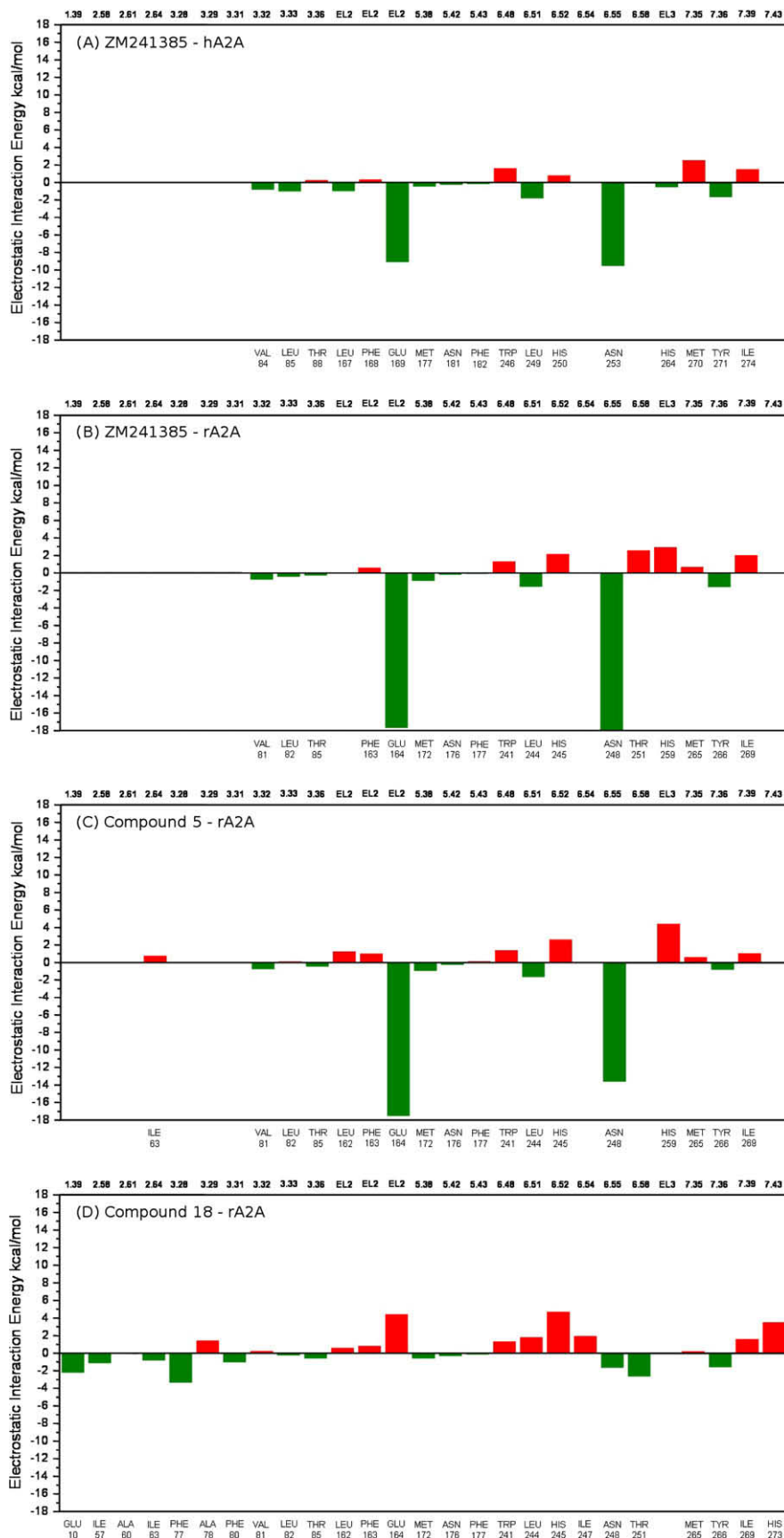


Figure 4. Electrostatic interaction energy (in kcal/mol) between the ligand and each single amino acid involved in ligand recognition calculated from: (A) crystallographic binding mode of ZM241385 inside the hA_{2A} receptor (PDB code: 3EML); (B) hypothetical binding mode of ZM241385 inside the rA_{2A} receptor obtained after docking simulations; (C) hypothetical binding mode of compound **5** inside the rA_{2A} receptor obtained after docking simulations; and (D) hypothetical binding mode of compound **18** inside the rA_{2A} receptor obtained after docking simulations.

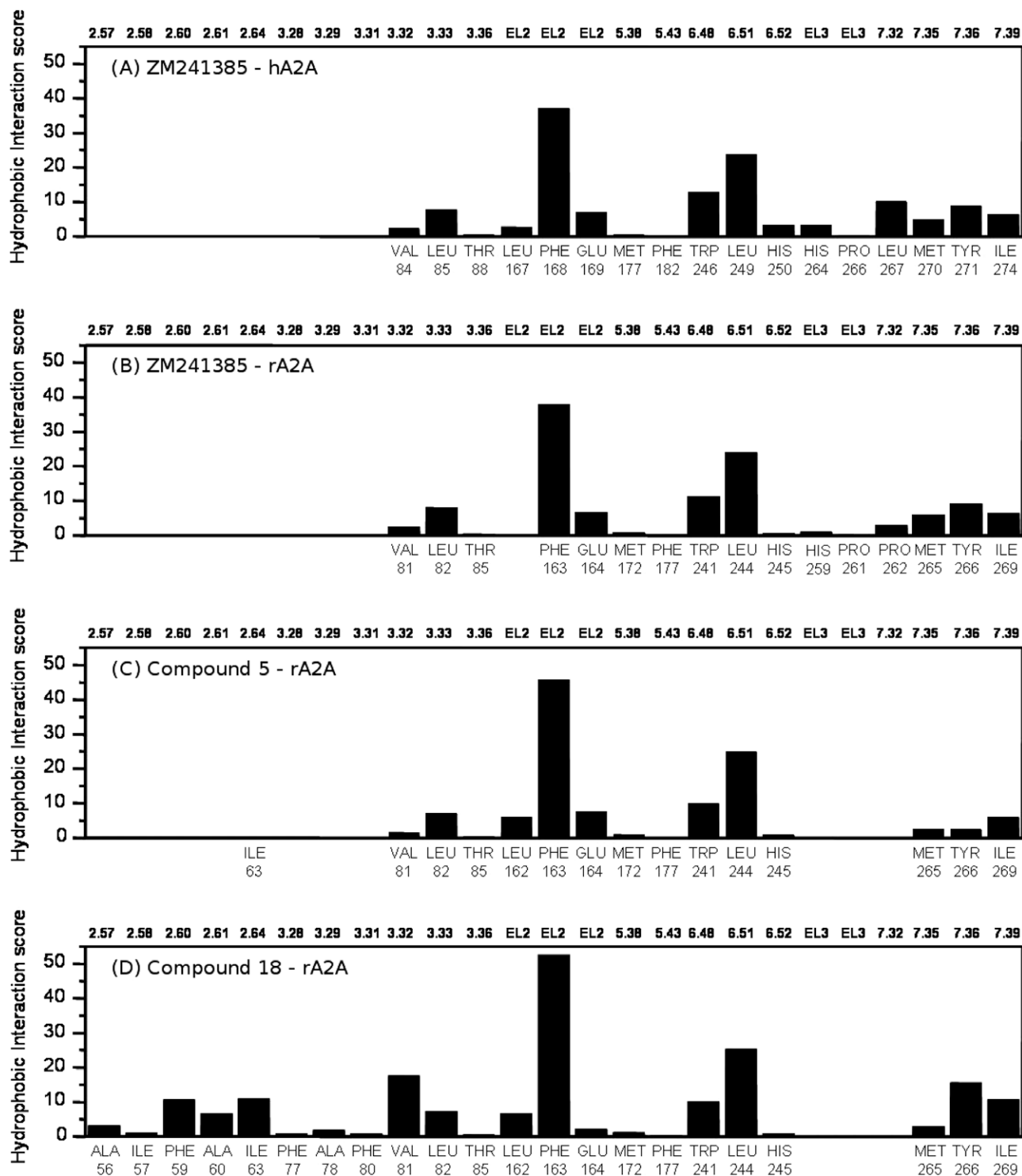


Figure 5. Hydrophobic interaction energy (in arbitrary hydrophobic unit) between the ligand and each single amino acid involved in ligand recognition calculated from: (A) crystallographic binding mode of ZM241385 inside the hA_{2A} receptor (PDB code: 3EML); (B) hypothetical binding mode of ZM241385 inside the rA_{2A} receptor obtained after docking simulations; (C) hypothetical binding mode of compound **5** inside the rA_{2A} receptor obtained after docking simulations; and (D) hypothetical binding mode of compound **18** inside the rA_{2A} receptor obtained after docking simulations.

(7) as a pale yellow solid in a good yield (80%). Mp 260–262 °C (EtOAc–light petroleum); IR (KBr): 3300, 1620, 1510 cm⁻¹; ¹H NMR (DMSO-*d*₆) δ: 3.1 (s, 6H); 6.7 (dd, 1H, *J* = 2, *J* = 4), 7.1 (d, 1H, *J* = 2); 7.9 (d, 1H, *J* = 4); 8.2 (br s, 2H). MW 245.24. Anal. Calcd for C₁₀H₁₁N₇O: C, 48.98; H, 4.52; N, 39.98. Found: C, 49.15; H, 4.50; N, 39.77.

4.1.2. General procedure for the preparation of the 7-(aralkyl-carbonyl)amino-2-(2-furyl)-5-substituted[1,2,4]triazolo[1,5-*a*][1,3,5]triazine derivatives (**8–11**, **14–17**, **20–23**)

A solution of amino derivative (**5–7**) (1 mmol), appropriate acyl chloride (1.2 equiv) and triethylamine (1.2 equiv) in dry dioxane (10 mL) was poured at reflux under argon atmosphere for 12 h.

The solvent was removed in vacuo, and the crude residue purified by flash chromatography (EtOAc–light petroleum 3:7) to afford the desired compound.

4.1.2.1. 7-Diphenyl-acetylamino-2-(2-furyl)-5-methylthio[1,2,4]-triazolo[1,5-a]-[1,3,5]triazine (8). Yield 65%; pale yellow solid; mp 172–173 °C (EtOAc–light petroleum); IR (KBr): 1680, 1520, 1420 cm^{-1} ; ^1H NMR (DMSO- d_6) δ : 2.53 (s, 3H); 5.1 (s, 1H); 6.7 (dd, 1H, $J = 2, J = 4$); 7.1 (d, 1H, $J = 2$); 7.2–7.6 (m, 10H); 7.9 (d, 1H, $J = 4$); 9.87 (br s, 1H). MW 442.49. Anal. Calcd for $\text{C}_{23}\text{H}_{18}\text{N}_6\text{O}_2\text{S}$: C, 62.43; H, 4.10; N, 18.99. Found: C, 62.66; H, 4.18; N, 19.13.

4.1.2.2. 2-(2-Furyl)-5-methylthio-7-phenylacetylamino-[1,2,4]-triazolo[1,5-a]-[1,3,5]triazine (9). Yield 75%; brown solid; mp 70–72 °C (EtOAc–light petroleum); IR (KBr): 1680, 1510, 1450 cm^{-1} ; ^1H NMR (DMSO- d_6) δ : 2.51 (s, 3H); 4.0 (s, 2H); 6.7 (dd, 1H, $J = 2, J = 4$); 7.1 (d, 1H, $J = 2$); 7.2–7.6 (m, 5H); 7.9 (d, 1H, $J = 4$); 11.8 (br s, 1H). MW 366.40. Anal. Calcd for $\text{C}_{17}\text{H}_{14}\text{N}_6\text{O}_2\text{S}$: C, 55.73; H, 3.85; N, 22.94. Found: C, 55.63; H, 3.79; N, 22.90.

4.1.2.3. 2-(2-Furyl)-7-[4-(methoxyphenyl)acetyl]amino-5-methylthio [1,2,4]triazolo[1,5-a][1,3,5]triazine (10). Yield 78%; pale yellow; mp 138–141 °C (EtOAc–light petroleum); IR (KBr): 1680, 1525, 1455 cm^{-1} ; ^1H NMR (DMSO- d_6) δ : 2.5 (s, 3H); 3.8 (s, 3H); 4.3 (s, 3H); 4.5 (s, 2H); 6.7 (dd, 1H, $J = 2, J = 4$); 6.9 (d, 2H, $J = 9$); 7.1 (d, 1H, $J = 2$); 7.2 (d, 2H, $J = 9$); 7.9 (d, 1H, $J = 4$); 11.8 (br s, 1H). MW 396.42. Anal. Calcd for $\text{C}_{18}\text{H}_{16}\text{N}_6\text{O}_3\text{S}$: C, 54.54; H, 4.07; N, 21.20. Found: C, 54.70; H, 4.11; N, 21.08.

4.1.2.4. 2-(2-Furyl)-5-methylthio-7-n-pentylcarbonylamino- [1,2,4]-triazolo[1,5-a]-[1,3,5]triazine (11). Yield 70%; white solid; mp 125–127 °C (EtOAc–light petroleum); IR (KBr): 1675, 1520, 1450 cm^{-1} ; ^1H NMR (DMSO- d_6) δ : 0.91 (t, 3H, $J = 7$); 1.01–1.2 (m, 4H); 1.4–1.61 (m, 2H); 2.5 (s, 3H); 3.32 (t, 2H, $J = 7$); 6.7 (dd, 1H, $J = 2, J = 4$); 7.1 (d, 1H, $J = 2$); 7.9 (d, 1H, $J = 4$); 10.93 (br s, 1H). MW 346.41. Anal. Calcd for $\text{C}_{15}\text{H}_{18}\text{N}_6\text{O}_2\text{S}$: C, 52.01; H, 5.24; N, 24.26. Found: C, 52.15; H, 5.20; N, 24.07.

4.1.2.5. 7-Diphenylacetylamino-2-(2-furyl)-5-phenoxy[1,2,4]-triazolo[1,5-a]-[1,3,5]triazine (14). Yield 67%; pale yellow solid; mp 136–139 °C (EtOAc–light petroleum); IR (KBr): 1680, 1520, 1425 cm^{-1} ; ^1H NMR (DMSO- d_6) δ : 5.12 (s, 1H); 6.73 (dd, 1H, $J = 2, J = 4$); 7.1 (d, 1H, $J = 2$); 7.2–7.6 (m, 15H); 7.9 (d, 1H, $J = 4$); 10.15 (br s, 1H). MW 488.50. Anal. Calcd for $\text{C}_{28}\text{H}_{20}\text{N}_6\text{O}_3$: C, 68.84; H, 4.13; N, 17.20. Found: C, 68.91; H, 4.21; N, 17.08.

4.1.2.6. 2-(2-Furyl)-5-phenoxy 7-phenylacetylamino- [1,2,4]triazolo[1,5-a]-[1,3,5]triazine (15). Yield 65%; white solid; mp 208–210 °C (EtOAc–light petroleum); IR (KBr): 1680, 1520, 1425 cm^{-1} ; ^1H NMR (DMSO- d_6) δ : 4.2 (s, 2H); 6.7 (dd, 1H, $J = 2, J = 4$); 7.1 (d, 1H, $J = 2$); 7.2–7.6 (m, 10H); 7.9 (d, 1H, $J = 4$); 11.01 (br s, 1H). MW 412.40. Anal. Calcd for $\text{C}_{22}\text{H}_{16}\text{N}_6\text{O}_3$: C, 64.07; H, 3.91; N, 20.38. Found: C, 64.23; H, 3.88; N, 20.28.

4.1.2.7. 2-(2-Furyl)-7-[4-(methoxyphenyl)acetyl]amino-5-phenoxy[1,2,4]triazolo[1,5-a]-[1,3,5]triazine (16). Yield 70%; white solid; mp 178–181 °C (EtOAc–light petroleum); IR (KBr): 1680, 1525, 1455 cm^{-1} ; ^1H NMR (DMSO- d_6) δ : 3.8 (s, 3H); 4.2 (s, 2H); 6.73 (dd, 1H, $J = 2, J = 4$); 7.12 (d, 1H, $J = 2$); 7.2–7.45 (m, 7H); 7.62 (d, 2H, $J = 9$); 7.9 (d, 1H, $J = 4$); 10.77 (br s, 1H). MW 442.43. Anal. Calcd for $\text{C}_{23}\text{H}_{18}\text{N}_6\text{O}_4$: C, 62.44; H, 4.10; N, 19.00. Found: C, 62.28; H, 4.15; N, 18.89.

4.1.2.8. 2-(2-Furyl)-7-n-pentylcarbonylamino-5-phenoxy[1,2,4]-triazolo[1,5-a]-[1,3,5]triazine (17). Yield 71%; white solid; mp 157–159 °C (EtOAc–light petroleum); IR (KBr): 1685, 1515,

1450 cm^{-1} ; ^1H NMR (DMSO- d_6) δ : 0.93 (t, 3H, $J = 7$); 1.05–1.19 (m, 4H); 1.43–1.65 (m, 2H); 3.35 (t, 2H, $J = 7$); 6.68 (dd, 1H, $J = 2, J = 4$); 7.21 (d, 1H, $J = 2$); 7.35–7.63 (m, 5H); 7.94 (d, 1H, $J = 4$); 10.58 (br s, 1H). MW 392.41. Anal. Calcd for $\text{C}_{20}\text{H}_{20}\text{N}_6\text{O}_3$: C, 61.21; H, 5.14; N, 21.42. Found: C, 61.53; H, 5.23; N, 21.58.

4.1.2.9. 5-Dimethylamino-7-diphenylacetylamino-2-(2-furyl)-[1,2,4]triazolo[1,5-a]-[1,3,5]triazine (20). Yield 70%; yellow solid; mp 105–107 °C (EtOAc–light petroleum); IR (KBr): 1680, 1520, 1425 cm^{-1} ; ^1H NMR (DMSO- d_6) δ : 3.13 (s, 6H); 4.32 (s, 1H); 6.68 (dd, 1H, $J = 2, J = 4$); 7.21 (d, 1H, $J = 2$); 7.32–7.65 (s, 10H); 7.88 (d, 1H, $J = 4$); 10.12 (br s, 1H). MW 439.47. Anal. Calcd for $\text{C}_{24}\text{H}_{21}\text{N}_7\text{O}_2$: C, 65.59; H, 4.82; N, 22.31. Found: C, 65.77; H, 4.82; N, 22.43.

4.1.2.10. 5-Dimethylamino-2-(2-furyl)-7-phenylacetylamino-[1,2,4]triazolo[1,5-a]-[1,3,5]triazine (21). Yield 75%; yellow solid; mp 226–228 °C (EtOAc–light petroleum); IR (KBr): 1680, 1525, 1455 cm^{-1} ; ^1H NMR (DMSO- d_6) δ : 3.15 (s, 6H); 4.28 (s, 2H); 6.69 (dd, 1H, $J = 2, J = 4$); 7.08 (d, 1H, $J = 2$); 7.4–7.55 (m, 5H); 7.85 (d, 1H, $J = 4$); 11.02 (br s, 1H). MW 363.37. Anal. Calcd for $\text{C}_{18}\text{H}_{17}\text{N}_7\text{O}_2$: C, 59.50; H, 4.72; N, 26.98. Found: C, 59.68; H, 4.71; N, 26.75.

4.1.2.11. 5-Dimethylamino-2-(2-furyl)-7-[4-(methoxyphenyl)-acetyl]amino-[1,2,4]triazolo[1,5-a]-[1,3,5]triazine (22). Yield 73%; pale yellow solid; mp 168–171 °C (EtOAc–light petroleum); IR (KBr): 1680, 1530, 1460 cm^{-1} ; ^1H NMR (DMSO- d_6) δ : 3.09 (s, 6H); 3.88 (s, 3H); 4.45 (s, 2H); 6.73 (dd, 1H, $J = 2, J = 4$); 7.12 (d, 1H, $J = 2$); 7.18 (d, 2H, $J = 9$); 7.47 (d, 2H, $J = 9$); 7.85 (d, 1H, $J = 4$); 10.43 (br s, 1H). MW 393.41. Anal. Calcd for $\text{C}_{19}\text{H}_{19}\text{N}_7\text{O}_3$: C, 58.01; H, 4.87; N, 24.92. Found: C, 57.78; H, 4.74; N, 24.83.

4.1.2.12. 5-Dimethylamino-2-(2-furyl)-7-n-pentylcarbonylamino-[1,2,4]triazolo[1,5-a]-[1,3,5]triazine (23). Yield 68%; white solid; mp 147–148 °C (EtOAc–light petroleum); IR (KBr): 1685, 1515, 1450 cm^{-1} ; ^1H NMR (DMSO- d_6) δ : 0.89 (t, 3H, $J = 7$); 0.99–1.05 (m, 4H); 1.32–1.55 (m, 2H); 3.14 (s, 6H); 3.29 (t, 2H, $J = 7$); 6.72 (dd, 1H, $J = 2, J = 4$); 7.15 (d, 1H, $J = 2$); 7.86 (d, 1H, $J = 4$); 10.04 (br s, 1H). MW 343.38. Anal. Calcd for $\text{C}_{16}\text{H}_{21}\text{N}_7\text{O}_2$: C, 55.96; H, 6.16; N, 28.55. Found: C, 56.13; H, 6.23; N, 28.73.

4.1.3. General procedure for the preparation of the 7-(arylcabamoyl)amino-2-(2-furyl)-5-substituted[1,2,4]triazolo[1,5-a]-[1,3,5]triazine derivatives (12, 13, 18, 19, 24, 25)

A solution of amino compound (1 mmol) (5–7), appropriate isocyanate (1.2 equiv) in dry dioxane was refluxed under argon for 18 h. The solvent was removed in vacuo, and the crude product was purified by flash chromatography (EtOAc–light petroleum 4:6) to afford the final compound (12, 13, 18, 19, 24, 25).

4.1.3.1. 2-(2-Furyl)-5-methylthio-7-(phenylcarbonyl)amino-[1,2,4]triazolo[1,5-a]-[1,3,5]triazine (12). Yield 75%; yellow solid; mp 165–167 °C (EtOAc–light petroleum); IR (KBr): 1660, 1510, 1450 cm^{-1} ; ^1H NMR (DMSO- d_6) δ : 2.54 (s, 3H); 6.65 (dd, 1H, $J = 2, J = 4$); 7.13 (d, 1H, $J = 2$); 7.25–7.54 (m, 5H); 7.92 (d, 1H, $J = 4$); 8.76 (br s, 1H); 11.55 (br s, 1H). MW 367.39. Anal. Calcd for $\text{C}_{16}\text{H}_{13}\text{N}_7\text{O}_2\text{S}$: C, 52.31; H, 3.57; N, 26.29. Found: C, 52.45; H, 3.63; N, 26.61.

4.1.3.2. 2-(2-Furyl)-7-[4-methyl(phenylcarbonyl)]amino-5-methylthio [1,2,4]triazolo[1,5-a]-[1,3,5]triazine (13). Yield 69%; yellow solid; mp 169–171 °C (EtOAc–light petroleum); IR (KBr): 1665, 1525, 1450 cm^{-1} ; ^1H NMR (DMSO- d_6) δ : 2.28 (s, 3H); 2.55 (s, 3H); 6.66 (dd, 1H, $J = 2, J = 4$); 7.07 (d, 1H, $J = 2$); 7.23 (d, 2H, $J = 9$); 7.65 (d, 2H, $J = 9$); 7.83 (d, 1H, $J = 4$); 8.32 (br

s, 1H); 11.03 (br s, 1H). MW 381.41. Anal. Calcd for $C_{17}H_{15}N_7O_2S$: C, 53.53; H, 3.96; N, 25.71. Found: C, 53.57; H, 3.90; N, 25.59.

4.1.3.3. 2-(2-Furyl)-5-phenoxy-7-(phenylcarbamoyl)amino[1,2,4]-triazolo[1,5-a]-[1,3,5]triazine (18). Yield 65%; pale yellow solid; mp 196–198 °C (EtOAc–light petroleum); IR (KBr): 1658, 1509, 1455 cm^{-1} ; 1H NMR (DMSO- d_6) δ : 6.62 (dd, 1H, $J = 2, J = 4$), 7.03 (d, 1H, $J = 2$); 7.2–7.6 (m, 10H); 7.85 (d, 1H, $J = 4$); 8.77 (br s, 1H); 10.78 (br s, 1H). MW 414.39. Anal. Calcd for $C_{21}H_{15}N_7O_3$: C, 61.01; H, 3.66; N, 23.72. Found: C, 61.25; H, 3.72; N, 23.85.

4.1.3.4. 2-(2-Furyl)-7-[4-methyl(phenylcarbamoyl)]amino-5-phenoxy[1,2,4]triazolo[1,5-a]-[1,3,5]triazine (19). Yield 73%; pale yellow solid; mp 203–205 °C (EtOAc–light petroleum); IR (KBr): 1668, 1530, 1465 cm^{-1} ; 1H NMR (DMSO- d_6) δ : 2.31 (s, 3H); 6.71 (dd, 1H, $J = 2, J = 4$), 7.12 (d, 1H, $J = 2$); 7.23–7.45 (m, 7H); 7.57 (d, 2H, $J = 9$); 7.86 (d, 1H, $J = 4$); 8.45 (br s, 1H); 10.08 (br s, 1H). MW 427.42. Anal. Calcd for $C_{22}H_{17}N_7O_3$: C, 61.82; H, 4.01; N, 22.94. Found: C, 62.01; H, 4.13; N, 23.07.

4.1.3.5. 5-Dimethylamino-2-(2-furyl)-7-(phenylcarbamoyl)amino-1,2,4-triazolo[1,5-a]-[1,3,5]triazine (24). Yield 80%; white solid; mp 270–274 °C (EtOAc–light petroleum); IR (KBr): 1665, 1515, 1460 cm^{-1} ; 1H NMR (DMSO- d_6) δ : 3.14 (s, 6H); 6.70 (dd, 1H, $J = 2, J = 4$), 7.09 (d, 1H, $J = 2$); 7.34–7.58 (m, 5H); 7.89 (d, 1H, $J = 4$); 8.32 (br s, 1H); 10.65 (br s, 1H). MW 364.40. Anal. Calcd for $C_{17}H_{16}N_8O_2$: C, 56.04; H, 4.43; N, 30.75. Found: C, 56.21; H, 4.38; N, 30.58.

4.1.3.6. 5-Dimethylamino-2-(2-furyl)-7-[4-methyl(phenylcarbamoyl)]amino-1,2,4-triazolo[1,5-a]-[1,3,5]triazine (25). Yield 83%; white solid; mp 263–266 °C (EtOAc–light petroleum); IR (KBr): 1665, 1520, 1455 cm^{-1} ; 1H NMR (DMSO- d_6) δ : 2.24 (s, 3H); 3.16 (s, 6H); 6.69 (dd, 1H, $J = 2, J = 4$), 7.11 (d, 1H, $J = 2$); 7.24 (d, 2H, $J = 9$); 7.58 (d, 2H, $J = 9$); 7.86 (d, 1H, $J = 4$); 8.76 (br s, 1H); 11.03 (br s, 1H). MW 378.39. Anal. Calcd for $C_{18}H_{18}N_8O_2$: C, 57.74; H, 4.79; N, 29.61. Found: C, 57.35; H, 4.77; N, 29.78.

4.2. Biological activity

4.2.1. Radioligand binding to rA_1 and rA_{2A} ARs

Procedures for preparation of rat brain membranes were reported previously.^{44,45} For binding experiments, membranes were frozen and stored at -20 °C for ≤ 2 months. Adenosine deaminase (ADA) was from Boehringer Mannheim (Indianapolis, IN), [3H]R-PIA was from Amersham (Arlington Heights, IL), and [3H]CGS 21680 was from DuPont NEN (Boston, MA).

Binding of [3H]R-PIA to the A_1 AR from rat cortical membranes and of [3H]CGS 21680 to the A_{2A} AR from rat striatal membranes was performed as described previously.⁴⁶ Adenosine deaminase (ADA, 2 units/mL) was present during the preparation of brain membranes. Additional ADA was not added during incubation with the radioligand.

4.2.2. Radioligand binding to hA_3 ARs

[^{125}I]-AB-MECA was utilized in radioligand binding assays to membranes prepared from CHO cells expressing recombinant hA_3 ARs, as previously described.³⁶ ADA (3 units/mL) was present during the preparation of the membranes, in a preincubation of 30 min at 30 °C, and during the incubation with the radioligands. All nonradioactive compounds were initially dissolved in DMSO and diluted with buffer to the final concentration, where the amount of DMSO never exceeded 2%. Incubations were terminated by rapid filtration over Whatman GF/B filters, using a Brandell cell harvester (Brandell, Gaithersburg, MD). The tubes were rinsed three times with 3 mL of buffer each. At least six different concen-

trations of competitor, spanning 3 orders of magnitude adjusted appropriately for the IC_{50} of each compound, were used. IC_{50} values, calculated with the nonlinear regression method implemented in Graph-Pad (Prism, San Diego, CA), were converted to dissociation constants (K_i) as described.⁴⁷ Hill coefficients of the tested compounds were in the range of 0.8–1.1.

4.2.3. Adenylyl cyclase activity

Due to the lack of a suitable radioligand the affinity of antagonists and the relative potency of agonists at A_{2B} ARs was determined in adenylyl cyclase experiments. The procedure was carried out as described previously^{37,38} with minor modifications. Membranes were incubated with about 150,000 cpm of [α - ^{32}P]ATP for 20 min in the incubation mixture as described^{37,38} without EGTA and NaCl. For agonists the EC_{50} -values for the stimulation of adenylyl cyclase were calculated with the Hill equation. Hill coefficients in all experiments were near unity. IC_{50} values for concentration-dependent inhibition of NECA-stimulated adenylyl cyclase caused by antagonists were calculated accordingly. K_i values for antagonists were then calculated with the Cheng and Prusoff equation.⁴⁸

4.3. Computational methodologies

All modeling studies were carried out on a 20 CPU (Intel CoreTM2 Quad CPU 2.40 GHz) linux cluster. Homology modeling, energy calculation, and analyses of docking poses were performed using the Molecular Operating Environment (MOE, version 2008.10) suite.⁴⁹ The software package MOPAC (version 7),⁵⁰ implemented in MOE suite, was utilized for all quantum mechanical calculations. Docking simulations were performed using GOLD suite.⁵¹ Log P values were calculated using ACDLABS 10.0.⁵²

4.3.1. Homology model of rA_{2A} AR and hA_3 AR

Based on the assumption that GPCRs share similar TM boundaries and overall topology, homology models of the ARs were constructed. First, the amino acid sequences of TM helices of rA_{2A} and hA_3 receptor were aligned with those of hA_{2A} AR,³⁹ guided by the highly conserved amino acid residues, including the DRY motif (Asp3.49, Arg3.50, and Tyr3.51) and three proline residues (Pro4.60, Pro6.50, and Pro7.50) in the TM segments of GPCRs. The same boundaries were applied for the TM helices of rA_{2A} and hA_3 ARs as they were identified from the X-ray crystal structure for the corresponding sequences of hA_{2A} AR,³⁹ the C_R coordinates of which were used to construct the seven TM helices for the rA_{2A} and hA_3 ARs. The loop domains were constructed by the loop search method implemented in MOE on the basis of the structure of compatible fragments found in the Protein Data Bank. In particular, loops were modeled first in random order. For each loop, a contact energy function analyzes the list of candidates collected in the segment searching stage, taking into account all atoms already modeled and any atoms specified by the user as belonging to the model environment. These energies were then used to make a Boltzmann-weighted choice from the candidates, the coordinates of which were then copied to the model. Any missing side chain atoms were modeled using the same procedure. Side chains are modeled using a library of rotamers generated by systematic clustering of the Protein Data Bank data, using the same procedure. Side chains belonging to residues whose backbone coordinates were copied from a template were modeled first, followed by side chains of modeled loops. Outgaps and their side chains were modeled last. Special caution has to be given to the second extracellular loop (EL2) because amino acids of this loop could be involved in direct interactions with the ligands. A driving force to this peculiar fold of the EL2 loop might be the presence of a disulfide bridge between cysteines in TM3 and EL2. The constraints were applied

Table 2
Comparison of different molecular docking protocols

Docking protocol	Best RMSD (Å)	Best ranked pose RMSD (Å)	Mean poses RMSD (Å)	Number of poses with RMSD <2.5 Å
MOE tabù search	1.61	3.35	5.65	4/25
MOE simulated annealing	2.17	4.36	6.47	1/25
MOE genetic algorithm	2.25	9.06	6.66	2/25
GOLD (goldscore)	0.63	1.95	1.20	25/25
GOLD (chemscore)	1.31	3.90	3.13	11/25
GOLD (asp)	0.61	4.96	1.50	23/25
GLIDE	0.79	2.71	6.82	7/25
PLANTS (chemplp)	0.93	1.98	6.96	3/25
PLANTS (plp)	0.84	1.93	6.70	6/25
PLANTS (plp95)	1.97	11.80	8.22	4/25

before the construction of the homology model, in particular during the sequences alignment, selecting the cysteine residues involved in the disulfide bridge in hA_{2A} to be constrained with the corresponding cysteines in hA₃ sequence. In particular, Cys166 (EL2) in hA_{2A} was constrained with Cys166 (EL2) in hA₃ and Cys77 (3.25) in hA_{2A} with Cys83 (3.25) in hA₃. When performing the alignment, MOE-Align attempts to minimize the number of constraint violations. Then, after running the homology modeling, the presence of the conserved disulfide bridge in the model was manually checked. Since this covalent link was conserved in all ARs modeled in the current study, the EL2 loop was modeled using a hA_{2A}-like constrained geometry around the EL2-TM3 disulfide bridge. In rA_{2A} receptor all the three disulfide bridge that characterize the template were conserved; for this reason the loop was modeled constraining all its residues. After the heavy atoms were modeled, all hydrogen atoms were added and were then minimized with MOE using the AMBER99⁵³ force field. The minimizations were carried out by the 1000 steps of steepest descent followed by conjugate gradient minimization until the rms gradient of the potential energy was less than 0.1 kcal mol⁻¹ Å⁻¹. We used Protonate 3D methodology, part of the MOE suite, for protonation state assignment by selecting a protonation state for each chemical group that minimizes the total free energy of the system (taking titration into account).⁵⁴

Protein stereochemical evaluation was then performed using several tools (Ramachandran and Chi plots measure phi/psi and chi1/chi2 angles, clash contacts reports) implemented in MOE suite.⁴⁹

4.3.2. Molecular docking of rA_{2A} AR and hA₃ AR antagonists

Ligand structures were built using MOE-builder tool, part of the MOE suite,⁴⁹ and were subjected to MMFF94x⁵⁵ energy minimization until the rms of conjugate gradient was 0.05 kcal mol⁻¹ Å⁻¹. Charges were calculated using ESP methodology.

Four different programs have been used to calibrate our docking protocols: MOE-DOCK,⁴⁹ GOLD,⁵¹ GLIDE,⁵⁶ and PLANTS.⁵⁷

Therefore ZM241385 was re-docked to the crystal structure of the hA_{2A} AR (PDB code: 3EML) with different docking algorithms and scoring functions (see Table 2).

Each docking was performed automatically to the binding site of the hA_{2A} AR without any constraints and without the presence of water molecules. For all the different docking simulations, the center of the docking box or of the docking sphere was set in the same point (got from the experimental pose of ZM241385 inside the crystal structure of hA_{2A} AR) and the number of independent docking runs was set to 25. Then RMSD values between predicted and crystallographic positions of ZM241385 were calculated.

As shown in Table 2, for each docking result there is at least one pose in good agreement with the experimental binding mode (RMSD value <2.5 Å). These poses with lowest RMSD value differ

from the crystallographic pose of ZM241385 mainly for the position of the phenylethylamine chain, while the bicyclic triazolotriazine core is almost aligned. However, the mean RMSD value is quite high for the most part of the docking protocols tested except for GOLD. Docking performed with GOLD gives the lowest RMSD value, the lowest mean RMSD value and the highest number of poses with RMSD value <2.5 Å.

Based on the best docking performance, all antagonist structures were docked into the hypothetical TM binding site of the hA₃ AR and the rA_{2A} AR models, by using the dock tool part of the GOLD suite. Searching is conducted within a user-specified docking sphere, using the Genetic Algorithm protocol and the GoldScore scoring function. GOLD performs a user-specified number of independent docking runs (25 in our specific case) and writes the resulting conformations and their energies in a molecular database file. The resulting docked complexes were subjected to MMFF94x energy minimization until the rms of conjugate gradient was <0.1 kcal mol⁻¹ Å⁻¹. Charges for the ligands were imported from the MOPAC output files using PM3/ESP methodology.

Prediction of antagonist–receptor complex stability (in terms of corresponding pK_i value) and the quantitative analysis for non-bonded intermolecular interactions (H-bonds, transition metal, water bridges, hydrophobic, electrostatic) were calculated and visualized using several tools implemented in MOE suite.³⁹

Electrostatic and hydrophobic contributions to the binding energy of individual amino acids have been calculated based on the AMBER99 force field as implemented in MOE suite.³⁹ To estimate the electrostatic contributions, atomic charges for the ligands were calculated using PM3/ESP methodology; instead partial charges for protein amino acids were calculated based on the AMBER99 force field.

Acknowledgements

The molecular modeling work coordinated by S.M. was carried out with financial support from the University of Padova, Italy, and the Italian Ministry for University and Research (MIUR), Rome, Italy. S.M. is also very grateful to Chemical Computing Group for the scientific and technical partnership. This research was supported in part by the Intramural Research Program of the NIH, National Institute of Diabetes and Digestive and Kidney Diseases.

References and notes

- Downey, J. M.; Cohen, M. V.; Ytrehus, K.; Liu, Y. *Ann. N.Y. Acad. Sci.* **1994**, 723, 82.
- Auchampach, J. A.; Jin, X.; Wan, T. C.; Caughey, G. H.; Linden, J. *Mol. Pharmacol.* **1997**, 52, 846.
- Jacobson, K. A.; von Lubitz, D. K. J. E.; Daly, J. W.; Fredholm, B. B. *Trends Pharmacol. Sci.* **1996**, 17, 108.
- Fredholm, B. B. *Int. Rev. Neurobiol.* **1997**, 40, 259.
- Feoktistov, I.; Polosa, R.; Holgate, S. T.; Biaggioni, I. *Trends Pharmacol. Sci.* **1998**, 19, 148.

6. Fozard, J. R.; McCarthy, C. *Curr. Opin. Invest. Drugs* **2002**, *3*, 69.
7. Richardson, P. J.; Kase, H.; Jenner, P. G. *Trends Pharmacol. Sci.* **1997**, *18*, 338.
8. Ribeiro, J. A.; Sebastiao, A. M.; de Mendonca, A. *Prog. Neurobiol.* **2002**, *68*, 377.
9. Yan, L.; Burbiel, J. C.; Maass, A.; Muller, C. E. *Expert Opin. Emerg. Drugs* **2003**, *8*, 537.
10. Fredholm, B. B. *Drug News Perspect.* **2003**, *16*, 283.
11. Moro, S.; Spalluto, G.; Jacobson, K. A. *Trends Pharmacol. Sci.* **2005**, *26*, 44.
12. Fredholm, B. B.; Arslan, G.; Halldner, L.; Kull, B.; Schulte, G.; Wasserman, W. *Naunyn-Schmiedeberg's Arch. Pharmacol.* **2000**, *362*, 364.
13. Moro, S.; Gao, Z. G.; Jacobson, K. A.; Spalluto, G. *Med. Res. Rev.* **2006**, *26*, 131.
14. Baraldi, P. G.; Cacciari, B.; Romagnoli, R.; Spalluto, G.; Monopoli, A.; Ongini, E.; Varani, K.; Borea, P. A. *J. Med. Chem.* **2002**, *45*, 115.
15. Baraldi, P. G.; Cacciari, B.; Spalluto, G.; Bergonzoni, M.; Dionisotti, S.; Ongini, E.; Varani, K.; Borea, P. A. *J. Med. Chem.* **1998**, *41*, 2126.
16. Baraldi, P. G.; Cacciari, B.; Spalluto, G.; Pineda de las Infantas y Villatoro, M. J.; Zocchi, C.; Dionisotti, S.; Ongini, E. *J. Med. Chem.* **1996**, *39*, 1164.
17. Baraldi, P. G.; Cacciari, B.; Romagnoli, R.; Spalluto, G.; Klotz, K.-N.; Leung, E.; Varani, K.; Gessi, S.; Merighi, S.; Borea, P. A. *J. Med. Chem.* **1999**, *42*, 4473.
18. Baraldi, P. G.; Cacciari, B.; Romagnoli, R.; Spalluto, G.; Moro, S.; Klotz, K. N.; Leung, E.; Varani, K.; Gessi, S.; Merighi, S.; Borea, P. A. *J. Med. Chem.* **2000**, *43*, 4768.
19. Baraldi, P. G.; Cacciari, B.; Moro, S.; Spalluto, G.; Pastorin, G.; Da Ros, T.; Klotz, K.-N.; Varani, K.; Gessi, S.; Borea, P. A. *J. Med. Chem.* **2002**, *45*, 770.
20. Maconi, A.; Pastorin, G.; Da Ros, T.; Spalluto, G.; Gao, Z. G.; Jacobson, K. A.; Baraldi, P. G.; Cacciari, B.; Varani, K.; Borea, P. A. *J. Med. Chem.* **2002**, *45*, 3579.
21. Pastorin, G.; Da Ros, T.; Spalluto, G.; Deflorian, F.; Moro, S.; Cacciari, B.; Baraldi, P. G.; Gessi, S.; Varani, K.; Borea, P. A. *J. Med. Chem.* **2003**, *46*, 4287.
22. Pinna, A.; Volpini, R.; Cristalli, G.; Morelli, M. *Eur. J. Pharmacol.* **2005**, *512*, 157.
23. Vu, C. B.; Pan, D.; Peng, B.; Kumaravel, G.; Phadke, D.; Engber, T.; Huang, C.; Reilly, J.; Tam, S.; Petter, R. C. *Bioorg. Med. Chem. Lett.* **2004**, *14*, 4831.
24. Dowling, J. E.; Vessels, J. T.; Haque, S.; Chang, H. X.; van Vloten, K.; Kumaravel, G.; Engber, T. M.; Jin, X.; Phadke, D.; Wang, J.; Ayyub, E.; Petter, R. C. *Bioorg. Med. Chem. Lett.* **2005**, *15*, 4809.
25. Gang, Y.; Haque, S.; Sha, L.; Kumaravel, G.; Wang, J.; Engber, T. M.; Whalley, E. T.; Conlon, P. R.; Chang, H.; Kiesman, W. F.; Petter, R. C. *Bioorg. Med. Chem. Lett.* **2005**, *15*, 511.
26. Vu, C. B.; Shields, P.; Peng, B.; Kumaravel, G.; Jin, X.; Phadke, D.; Wang, J.; Engber, T.; Ayyub, E.; Petter, R. C. *Bioorg. Med. Chem. Lett.* **2004**, *14*, 4835.
27. Peng, B.; Kumaravel, G.; Yao, G.; Sha, L.; Van Vlijmen, H.; Bohnert, T.; Huang, C.; Vu, C. B.; Ensinger, C. L.; Chang, H.; Engber, T. M.; Whalley, E.; Petter, R. C. *J. Med. Chem.* **2004**, *47*, 6218.
28. Vu, C. B.; Pan, D.; Kumaravel, G.; Smits, G.; Jin, X.; Phadke, D.; Engber, T.; Huang, C.; Reilly, J.; Tam, S.; Grant, D.; Hetu, G.; Petter, R. C. *J. Med. Chem.* **2005**, *48*, 2009.
29. Poucher, S. M.; Keddie, J. R.; Singh, P.; Stoggall, S. M.; Caulkett, P. W. R.; Jones, G.; Collis, M. G. *Br. J. Pharmacol.* **1995**, *115*, 1096.
30. DeZwart, M.; Vollinga, R. C.; Beukers, M. W.; Slegers, D. F.; von Frijtag Drabbe Kunzel, J. K.; De Groot, M.; IJzerman, A. P. *Drug Dev. Res.* **1999**, *48*, 95.
31. Ji, X. D.; Jacobson, K. A. *Drug Des. Discovery* **1999**, *16*, 217.
32. Caulkett, P. W. R.; Jones, G.; McPartlin, M.; Renshaw, N. D.; Stewart, S. K.; Wright, B. J. *Chem. Soc., Perkin Trans. 1* **1995**, 801.
33. Schwabe, U.; Trost, T. *Naunyn-Schmiedeberg's Arch. Pharmacol.* **1980**, *313*, 179.
34. Jarvis, M. F.; Schutz, R.; Hutchison, A. J.; Do, E.; Sills, M. A.; Williams, M. J. *Pharmacol. Exp. Ther.* **1989**, *251*, 888.
35. Salvatore, C. A.; Jacobson, M. A.; Taylor, H. E.; Linden, J.; Johnson, R. G. *Proc. Natl. Acad. Sci. U.S.A.* **1993**, *90*, 10365.
36. Olah, M. E.; Gallo-Rodriguez, C.; Jacobson, K. A.; Stiles, G. L. *Mol. Pharmacol.* **1994**, *45*, 978.
37. Klotz, K. N.; Hessling, J.; Hegler, J.; Owman, C.; Kull, B.; Fredholm, B. B.; Lohse, M. J. *Naunyn-Schmiedeberg's Arch. Pharmacol.* **1998**, *357*, 1.
38. Klotz, K. N.; Cristalli, G.; Grifantini, M.; Vittori, S.; Lohse, M. J. *J. Biol. Chem.* **1985**, *260*, 14659.
39. Jaakola, V. P.; Griffith, M. T.; Hanson, M. A.; Cherezov, V.; Chien, E. Y. T.; Lane, J. R.; IJzerman, A. P.; Stevens, R. C. *Science* **2008**, *322*, 1211.
40. Cunha, R. A.; Constantino, M. D.; Ribeiro, J. A. *Br. J. Pharmacol.* **1997**, *122*, 1279.
41. Ongini, E.; Dionisotti, S.; Gessi, S.; Irenius, E.; Fredholm, B. B. *Naunyn-Schmiedeberg's Arch. Pharmacol.* **1999**, *359*, 7.
42. Ballesteros, J. A.; Weinstein, H. *Methods Neurosci.* **1995**, *25*, 366.
43. Audet, M.; Bouvier, M. *Nat. Chem. Biol.* **2008**, *4*, 397.
44. Gallo-Rodriguez, C.; Ji, X. D.; Melman, N.; Siegman, B. D.; Sanders, L. H.; Orlina, J.; Pu, Q. L.; Olah, M. E.; van Galen, P. J. M.; Stiles, G. L.; Jacobson, K. A. *J. Med. Chem.* **1994**, *37*, 636.
45. van Galen, P. J. M.; van Bergen, A. H.; Gallo-Rodriguez, C.; Melman, N.; Olah, M. E.; IJzerman, A. P.; Stiles, G. L.; Jacobson, K. A. *Mol. Pharmacol.* **1994**, *45*, 1101.
46. van Bergen, A.; van Galen, P. J. M.; Stiles, G. L.; Jacobson, K. A. ACS 206th National Meeting, Chicago, IL, August, 1993; Abstract MED1217.
47. Linden, J. J. *Cyclic Nucleotide Res.* **1982**, *8*, 163.
48. Cheng, Y. C.; Prusoff, H. R. *Biochem. Pharmacol.* **1973**, *22*, 3099.
49. MOE (Molecular Operating Environment), version 2008.10; software available from Chemical Computing Group Inc. (1010 Sherbrooke Street West, Suite 910, Montreal, Quebec, Canada H3A 2R7). <http://www.chemcomp.com>.
50. Stewart, J. J. P. *MOPAC 7*; Fujitsu Limited: Tokyo, Japan, 1993.
51. GOLD suite, version 4.0.1; software available from Cambridge Crystallographic Data Centre Cambridge Crystallographic Data Centre (12 Union Road Cambridge CB2 1EZ UK). <http://www.ccdc.cam.ac.uk>.
52. ACDLABS, version 10.0; software available from Advanced Chemistry Development, Inc. (110 Yonge Street, 14th floor, Toronto, Ontario, Canada M5C 1T4).
53. Cornell, W. D.; Cieplak, P.; Bayly, C. I.; Gould, I. R.; Merz, K. M.; Ferguson, D. M.; Spellmeyer, D. C.; Fox, T.; Caldwell, J. W.; Kollman, P. A. *J. Am. Chem. Soc.* **1995**, *117*, 5179.
54. Labute, P. *Proteins* **2009**, *75*, 187.
55. Halgren, T. J. *Comput. Chem.* **1996**, *17*, 490.
56. Halgren, T. A.; Myrphyl, R. B.; Friesner, R. A.; Beard, H. S.; Frye, L. L.; Pollard, W. T. *J. Med. Chem.* **2004**, *47*, 1739.
57. Korb, O.; Stützel, T.; Exner, T. E. *J. Chem. Inf. Model.* **2009**, *49*, 84.